

# An advanced study for defect disposition through 193nm aerial imaging

Arndt C. Dürr<sup>a\*</sup>, Axel M. Zibold<sup>b</sup>, Klaus Böhm<sup>b</sup>

<sup>a</sup>Advanced Mask Technology Center (AMTC), Rähnitzer Allee 9, 01109 Dresden, Germany

<sup>b</sup>Carl Zeiss SMS GmbH, Carl-Zeiss Promenade 10, 07745 Jena, Germany

## ABSTRACT

With decreasing structure sizes on masks also the acceptable CD variation corridor for printing on the wafer and therefore, the maximum allowed defect size is decreasing. This has not only implications to the accuracy and repeatability of front-end processes such as writers, etchers, etc. but also challenges defect inspection and qualification. Defect qualification is usually done by an AIMS<sup>TM</sup> tool which optically simulates the aerial image of the structures by applying the same illumination conditions as the wafer fabs' scanners. As lithographers continue to produce smaller and smaller structures, the acceptable variation pushes the AIMS<sup>TM</sup> evaluation step by step towards a metrology method. Thus, an advanced measurement capability of the AIMS<sup>TM</sup> tool is mandatory to reliably disposition defects within these small margins. It is influenced by the performance of illumination, imaging homogeneity, and stability. A possible measure for the tool's capability is the (long term) repeatability of the tool by evaluating the same defect with a certain frequency over several weeks. The AIMS<sup>TM</sup> fab 193i platform takes into account these increased requirements by improved optics such as a new beam homogenizer module, new energy monitoring and vibration isolation concept. In this paper we show data on the long term repeatability compared between the first generation AIMS<sup>TM</sup> fab 193SE and the new AIMS<sup>TM</sup> fab 193i platform and discuss the implications on the measurement capabilities of the two platforms.

**Keywords:** AIMS, defect disposition, aerial imaging, mask metrology, printability, automation, optical imaging, 193nm lithography, mask, reticle

## 1. INTRODUCTION

Mask making for the leading edge semiconductor industry has always been a challenge due to the "zero defect" requirements of the customers. Inspection of the masks and repair of defects are well established processes in mask shops to increase the production yield or – for advanced masks of the 90 nm node and below – make it even possible to meet the "zero defect" target, i.e. to deliver masks with only non-printing design variations. For defect disposition and (after-repair) qualification under stepper simulating optical illumination conditions AIMS tools are standard equipment in mask shops for over 10 years. With the decreasing structural sizes however, also the acceptable design variations are decreasing pushing the AIMS evaluation step by step towards a metrology method. This in turn imposes tighter hardware specifications to AIMS tools in order to meet the mask shops' stability needs. Key parameters for reliable defect dispositioning are

1. The pupil illumination homogeneity. AIMS measurements of the same mask in 0° and 90° orientation could be required due to boundary conditions like pellicle size or the mask's orientation during the inspection. As shown recently<sup>1</sup> a homogeneous pupil illumination is mandatory if the defect disposition should be independent on the mask's orientation.
2. Stability of the light intensity with time and within the illuminated area. During mask processing frequently one and the same mask location is measured several times within several days, in particular for advanced masks being exposed to complex repairs. A large variability in the AIMS illumination could lead to significantly different CD or transmission results of the same site at different times. This decreases the process window for repairs since the AIMS induced variance inherently decreases the customers' error margin.

---

\*Further author information: (Send correspondence to Arndt C. Dürr)  
E-mail: Arndt.Duerr@amtc-dresden.com, Telephone: +49 (0) 351 4048 268

The currently available AIMS fab 193i tool introduced by ZEISS to the market end of 2004 is a further development of a 2nd generation tool following the AIMS fab 193SE tool. The new AIMS fab 193i accounts particularly for the above mentioned subjects improving the pupil homogeneity and stability. On the new tool special attention was paid to the optical beam path. Key elements of the system are a 193nm excimer laser, a beam homogenizer, an illumination unit, an imaging unit and a CCD camera. A new beam homogenizer using special transmitting optical elements was developed ensuring a symmetrically homogenized and stable pupil uniformity. It allows to realize a balanced and stable intensity distribution even for small poles used for off-axis illumination in optical lithography. New manufacturing methods and alignment procedures including interferometric testing allow to build systems with reduced aberration level. These improvements are crucial for field and pupil uniformity specifications. A new energy monitoring system is realized and monitors the light energy within the illumination unit. It is a key element for providing system stability and improves significantly both short and long term measurement repeatability values. On the imaging side the dynamic measurement range was enlarged enabling an increase in throughput and tool productivity. Besides the optical performance and aerial image measurement improvements the AIMS fab 193i tools are highly automated and efficiently sensitive for production environments. The systems are optionally available with mini-environment, a robotic reticle handling system, SMIF interface, particle sensors, ionizer and can provide ISO 2 class compatibility on the reticle path. Other functional improvements are done such as a new exchange mechanism for off-axis pattern and new overview illumination capability for navigation purpose.

In this paper we will highlight the improvements of the new AIMS fab 193i tool by a detailed investigation of pupil illumination characteristics as well as by a stability analysis of repeated measurements and evaluation of the same structure over several days. These measurements are compared to a predecessor generation AIMS fab 193SE tool.

## 2. EXPERIMENTAL

For the investigation of pupil characteristics and the stability two 193 nm AIMS tools, an AIMS fab 193SE and an AIMS fab 193i were used.

### 2.1. Pupil Characterization

Following a recent study,<sup>1</sup> the pupil illumination can be characterized by a simple parameterization: “ellipticity” ( $E$ ), “pole balance X” ( $PBX$ , along its East-West axis), and “pole balance Y” ( $PBY$ , along its North-South axis). Figure 1 shows, how these parameters are defined by cutting the aperture in 4 sectors (“north”, “east”, “south”, and “west”) with their corresponding integrated intensities:  $I_N$ ,  $I_E$ ,  $I_S$ ,  $I_W$ :

$$E = \frac{(I_N + I_S) - (I_W + I_E)}{(I_N + I_S) + (I_W + I_S)} \times 100\% \quad (1)$$

$$PBX = \frac{I_W - I_E}{I_W + I_S} \times 100\% \quad (2)$$

$$PBY = \frac{I_N - I_S}{I_N + I_S} \times 100\% . \quad (3)$$

For the pupil characteristics test an “annular 66%” aperture with a numerical aperture ( $NA$ ) of  $NA = 0.7$  and  $\sigma_{out} = 0.8$  was used. This aperture was aligned by the the standard centering process “check pupil image” at a clear spot of production masks, imaged and subsequently analyzed by an algorithm developed in cooperation between ZEISS and AMTC with respect to  $E$ ,  $PBX$ , and  $PBY$ . To determine the variance of these pupil characteristics 10 pupil images were taken at each tool at different times and the average and the  $3\sigma$ -value of the parameters were calculated.

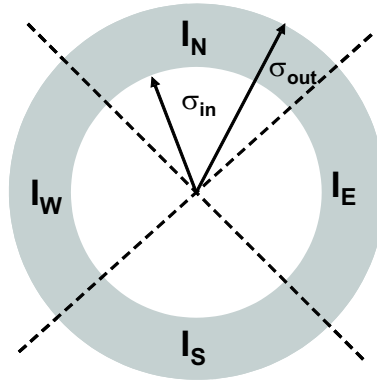


**Figure 1.** Sector parameterization of an annular illumination with integrated sector intensities for the calculation of the pupil characterization.

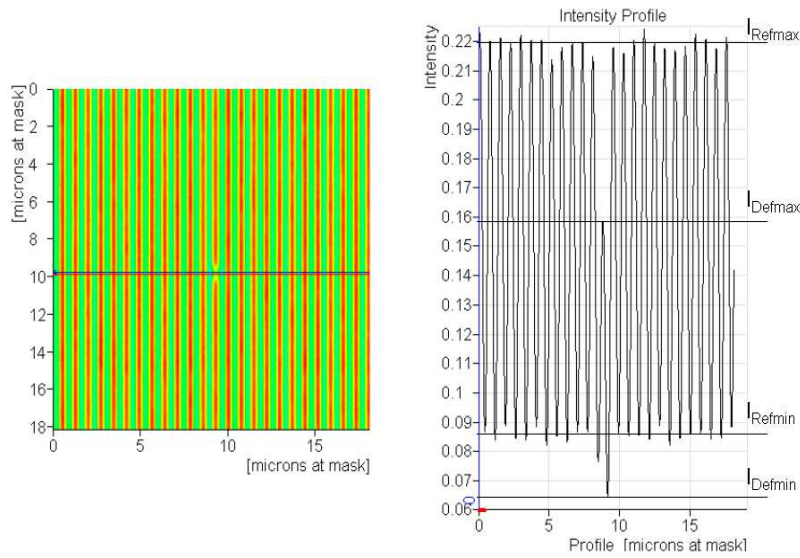


**Figure 2.** Typical l&s structure imaged by an AIMS tool and profile along the line (left-hand side). On the right hand side the intensity profile of this profile is displayed. The evaluation of  $I_{RefMax}$ ,  $I_{DefMax}$ ,  $I_{RefMin}$ , and  $I_{DefMin}$  is shown.

## 2.2. Stability measurements of defects

In this study, the defect and contrast evaluation is based on the transmission criterion, see Fig. 2. Hereby, the light intensity as determined using the AIMS software at the defective site (defect maximum  $I_{DefMax}$  and defect minimum  $I_{DefMin}$ , respectively) is referenced to a defect free site (reference maximum  $I_{RefMax}$  and reference minimum  $I_{RefMin}$ , respectively). These intensities are used to calculate the transmission deviation in the maximum ( $MaxTrans$ ), the transmission deviation in the minimum ( $MinTrans$ ), and the contrast ( $C$ ) by the following relations:

$$MaxTrans = \left(1 - \frac{I_{DefMax}}{I_{RefMax}}\right) \times 100\% \quad (4)$$

$$MinTrans = \frac{I_{DefMin} - I_{RefMin}}{I_{RefMax} - I_{RefMin}} \times 100\% \quad (5)$$

$$C = \frac{I_{RefMax} - I_{RefMin}}{I_{RefMax} + I_{RefMin}} \times 100\% . \quad (6)$$

To characterize the tools' stability over time a programmed defect in a lines-and-spaces (l&s) pattern on a halftone mask with a half-pitch of 100 nm (1x) was measured at more than ten different days. The average and the  $3\sigma$ -variance of  $C$ ,  $MaxTrans$ , and  $MinTrans$  of these measurements have been determined.

In addition the same defect has been imaged with the mask in  $0^\circ$  and  $90^\circ$  orientation, i.e. the l&s pattern in vertical and horizontal orientation, respectively. Subsequently, the differences of the pattern's contrast and of the defect printing behavior between both orientations have been calculated:  $\Delta C = |C_{=} - C_{||}|$ ,  $\Delta MaxTrans = |MaxTrans_{=} - MaxTrans_{||}|$ , and  $\Delta MinTrans = |MinTrans_{=} - MinTrans_{||}|$ , where the indices " $||$ " and " $=$ " refer to vertical and horizontal pattern orientation, respectively.

### 3. RESULTS AND DISCUSSION

#### 3.1. Pupil Homogeneity

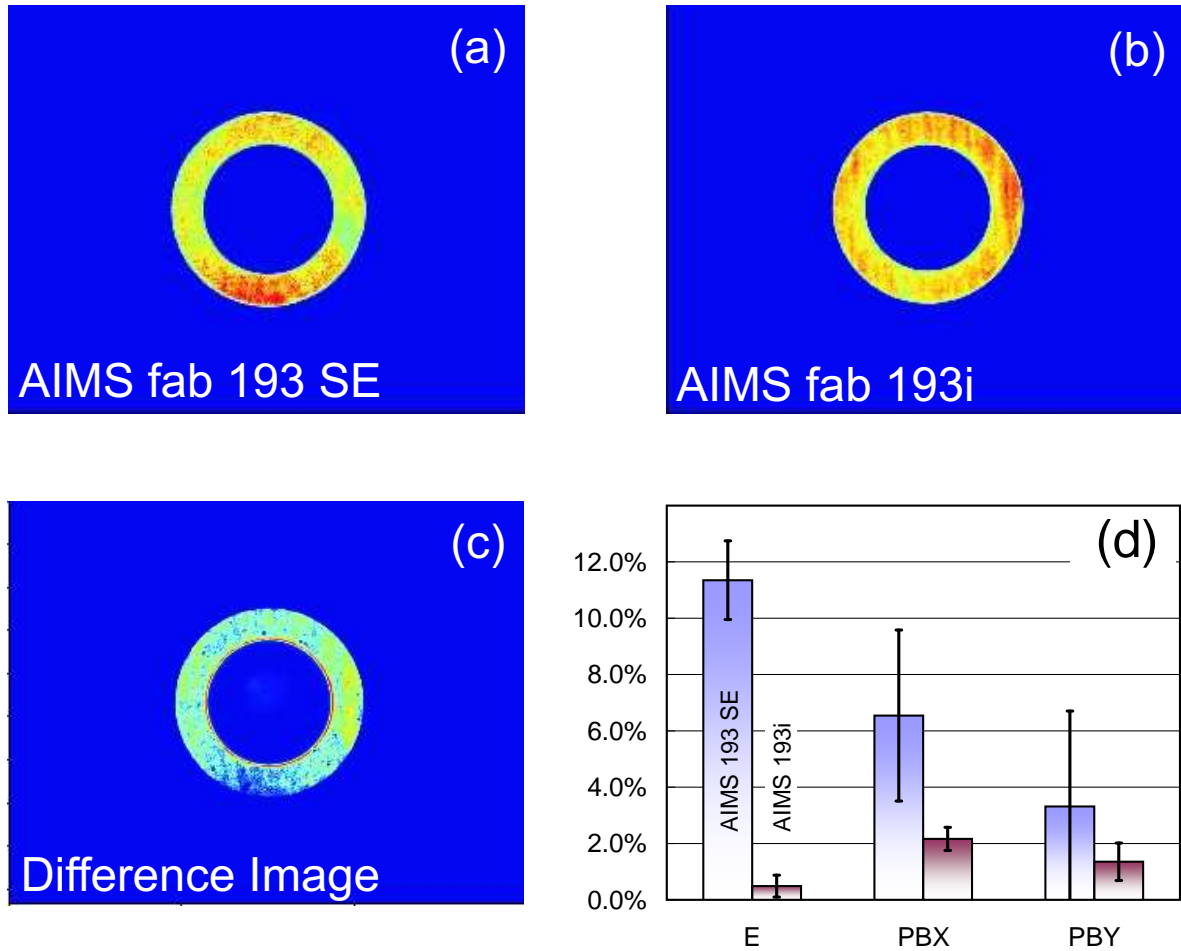
##### 3.1.1. Comparison of pupil characteristics and stability over time

Figure 3 shows annular 66% apertures at  $NA = 0.7$  and  $\sigma = 0.8$  imaged at the AIMS fab 193SE [Fig. 3(a)] and at the AIMS fab 193i [Fig. 3(b)], respectively, the difference image of both pupils (subtraction of the AIMS fab 193SE's pupil image from the AIMS fab 193i's pupil image) [Fig. 3(c)], and a diagram displaying the differences of the absolute pupil characteristics,  $E$ ,  $PBX$ , and  $PBY$  for both tools [Fig. 3(d)]. Average value and error bar ( $3\sigma$ -range) in Fig. 3(d) are obtained by the evaluation of 10 pupil images taken at 5 different days.

Comparing the pupil images of the AIMS fab 193SE and of the AIMS fab 193i [Figs. 3(a) and (b)] clearly demonstrates that the AIMS fab 193i shows a much more homogeneous pupil illumination. This can be attributed to the improved homogenizing concept of this tool. Closer inspection of the difference image [(pupil of AIMS fab 193i) - (pupil of AIMS fab 193SE)] in Fig. 3(c) reveals that the pupil of the investigated AIMS fab 193SE exhibits a pronounced intensity along its N-S axis compared to the AIMS fab 193i which will result in an larger contrast for horizontally oriented l&s-patterns compared to vertically oriented l&s-patterns. The quantitative evaluation of the pupil characteristics confirms the qualitative view of Figs. 3(a)-(c). The absolute values  $|E|$ ,  $|PBX|$ , and  $|PBY|$  of the AIMS fab 193SE are remarkably larger than the corresponding values of the AIMS fab 193i. The AIMS fab 193i exhibits for all regarded characteristics of the investigated aperture values close to or even below 2%. In addition, also the  $3\sigma$ -variability of the pupil characteristics is largely decreased compared to the AIMS fab 193SE being important for reproducible measurement results.

##### 3.1.2. Rotation matching

Rotation match experiments manifest the pupil homogeneity by imaging the exactly same l&s-pattern in horizontal and vertical orientation with the same aperture (see Section 2.2). Figure 4 shows the resulting differences  $\Delta C$ ,  $\Delta MaxTrans$ , and  $\Delta MinTrans$  of the rotation match experiment for both tools. In order to evaluate masks in both orientation in a production environment a difference close to zero in the rotation matching test is crucial to avoid misinterpretation of defects. The results are clear evidence for the improved capability of the AIMS fab 193i. All differences are clearly below 1%, for  $\Delta MaxTrans = 0.02\%$  and thus the bar in the graph is virtually not visible. *Note*, that the difference values are *absolute* values since the unit of all parameters is percent. The root cause for this improved capability is the better homogeneous pupil illumination homogeneity



**Figure 3.** Images and analysis of annular 66% apertures with  $NA = 0.7$  and  $\sigma = 0.8$ . (a) Aperture image of the AIMS fab 193SE. (b) Aperture image of the AIMS fab 193i. (c) Difference image of the aperture's of both tools: the aperture image of the AIMS fab 193SE is subtracted from the aperture image of the AIMS fab 193i. (d) Pupil characteristics ( $E$ ,  $PBX$ , and  $PBY$ ) of the aperture images from (a) and (b). For each parameter, the left hand (blue) bar depicts the characteristics of the AIMS fab 193SE whereas the right bar (red) depicts the characteristics of the AIMS fab 193i.

(see Section 3.1.1), but also the better vibration damping of the system may contribute to the observed improvement. As discussed in<sup>1</sup> an inhomogeneous pupil illumination, in particular a non-zero ellipticity, results in deviations of  $C$ ,  $MaxTrans$ , and  $MinTrans$  between orthogonal pattern orientations (horizontal vs. vertical). Also, vibrations on the system may decrease the contrast: if the vibration direction acts perpendicular to the pattern's orientation the intensity at the bright structures' site is decreased due to dark structures oscillating over their sites and the intensity at the dark structures sites is increased due to bright structures oscillating over their sites. As a result the pattern gets blurred and the contrast decreases. Hence, the improved vibration damping of the AIMS fab 193i may also help to decrease the rotation match differences even though it is – with this simple test – not possible to completely discriminate the influence of pupil homogeneity and vibrations.

### 3.2. Defect repeatability

A key measure to reliably disposition defects on tightly specified advanced masks with AIMS tools is the reproducibility of the defect disposition over time. Repeated measurements of the same defect on the same mask with the same AIMS settings over a given period of time allow to evaluate the time stability of the tool by calculating the average values of  $C$ ,  $MaxTrans$ , and  $MinTrans$  and their corresponding  $3\sigma$  variances. For the

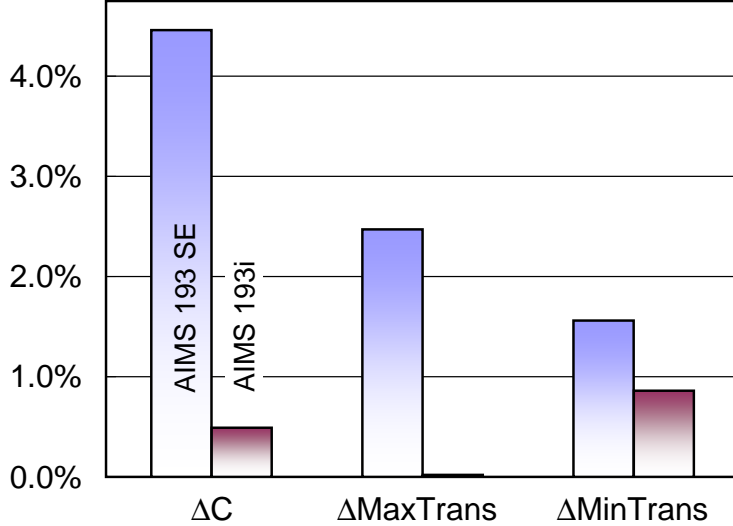


**Figure 4.** Results of the “rotation match” experiment.  $\Delta C$ ,  $\Delta MaxTrans$ , and  $\Delta MinTrans$  are displayed. For each parameter the values for the AIMS fab 193SE are depicted by the left bar (blue) and for the AIMS fab 193i by the right bar (red).

tight specification corridors of advanced masks it is crucial to keep the variance as low as possible to avoid errors such as (i) processing a mask with printing design variations further without repair having AIMS dispositioned the design variations as “in spec” and (ii) rejecting or re-repairing locations on masks that effectively are in specification having AIMS dispositioned these sites as “need repair”-sites. Figure 5 shows the results for repeatability measurements on the halftone mask with a half-pitch of 100 nm (1x) for both tools under investigation.

From top to bottom the differences in contrast  $\Delta C_i = C_i - \langle C \rangle$  [Figs. 5(a) and (b)], in transmission deviation in the maximum  $\Delta MaxTrans_i = MaxTrans - \langle MaxTrans \rangle$  [Figs. 5(c) and (d)], and transmission deviation in the minimum  $\Delta MinTrans_i = MinTrans - \langle MinTrans \rangle$  [Figs. 5(e) and (f)] are displayed, where the index  $i$  denotes the respective data point and  $\langle C \rangle$ ,  $\langle MaxTrans \rangle$ , and  $\langle MinTrans \rangle$  denote the average values of the three investigated parameters. The dotted horizontal lines depict the  $\pm 3\sigma$  range of the respective parameter and tool. The graphs on the left-hand side refer to the AIMS fab 193SE [Figs. 5(a), (c), (e)] and the graphs on the right-hand side refer to the AIMS fab 193i [Figs. 5(b), (d), (f)], respectively. *Note*, that all y-axes exhibit the same scaling range to allow for a direct comparison between both tools.

It is clearly seen that the variance of the AIMS fab 193i is reduced by a factor of  $> 2$  for all parameters compared to the AIMS fab 193SE. This can be attributed to the improved hardware of the AIMS fab 193 plus, namely the energy monitoring system and the homogeneizer unit. The energy monitor ensures that the cumulative energy for both clear-reference and patterned image acquisition is kept at a constant level on the the reticle illumination side. This results in reduced long term variations of the measurements. The homogeneizer itself reduces the variations within the image-field and enables an improved uniformity compared to the predecessor tool generation.

Figure 6 summarizes the  $3\sigma$  values of the various parameters for both tools. In addition, for the AIMS fab 193i, repeatability measurements for a halftone mask with a half-pitch of 75 nm (1x) are displayed (using a quasar aperture with  $NA = 0.8$  and  $\sigma = 0.92$ ). The results are similar to the results of the 100 nm (1x) halftone mask. This demonstrates a low variability-level of the AIMS fab 193i also for state-of-the-art production masks making the tool appropriately suited for reliable and reproducible defect disposition for all mask technologies which not yet require hyper-NA-illumination.

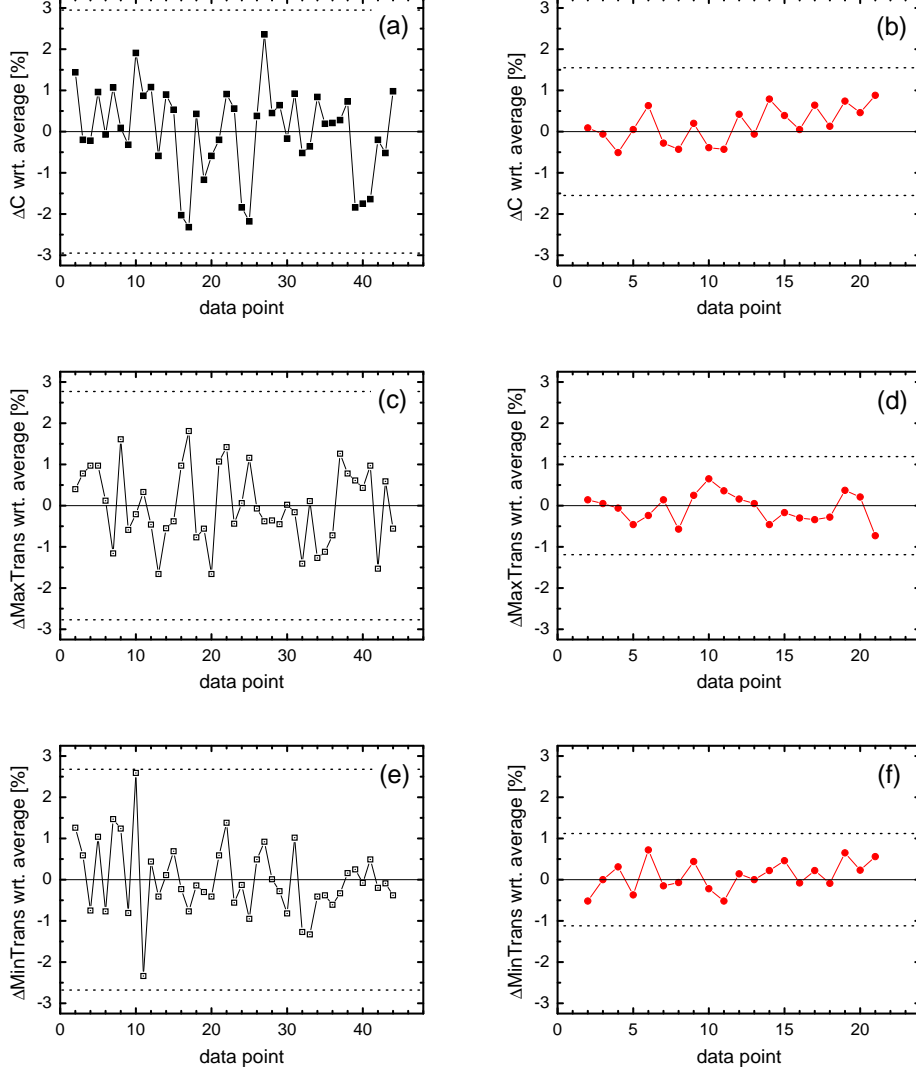


**Figure 5.** Repeated measurements of a programmed defect in a l&s pattern on a half-tone mask with a half-pitch of 100 nm (1x) over several days on an AIMS fab 193SE [left hand column, (a), (c), (e)] and on an AIMS fab 193i [right hand column, (b), (d), (f)], respectively. In all graphs the  $\pm 3\sigma$ -variance interval is displayed with dotted lines. (a) and (b): variation of  $C$  around the average value. (c) and (d) variation of  $MaxTrans$  around the average value. (e) and (f) variation of  $MinTrans$  around the average value. *Note*, that the y-scale is the same for each pair of measurements to allow for a direct comparison of the  $3\sigma$  range between both tools.

#### 4. SUMMARY AND CONCLUSIONS

In this study the performance of two 193 nm AIMS tools, the AIMS fab 193i and its predecessor, the AIMS fab 193SE, has been assessed and compared. Their pupil illumination homogeneity over time has been characterized in terms of the parameters  $E$ ,  $PBX$ , and  $PBY$ . Also, “rotation match” experiments have been carried out manifesting pupil inhomogeneities in AIMS measurements in a simple way. Long term repeatability measurements on a programmed defect on half-tone masks revealed the  $3\sigma$  variances of  $C$ , and of the defect evaluation variables  $MaxTrans$  and  $MinTrans$ , i.e. the stability of the tools over time. For all investigated measurements a considerably improved characteristic was observed for the AIMS fab 193i compared to the AIMS fab 193SE: The nearly

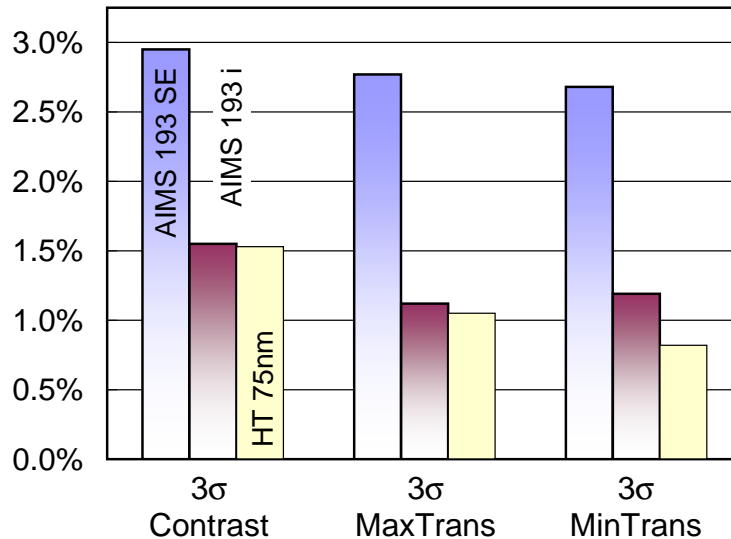


**Figure 6.**  $3\sigma$  values for  $C$ ,  $MaxTrans$ , and  $MinTrans$  of the AIMS fab 193SE (left hand column of each parameter) and of the AIMS fab 193i (middle and right hand column of each parameter) as determined by repeated measurements of a programmed defects mask over several days. The left hand and the middle column values refer to a halftone mask with a half-pitch of 100 nm (1x), the right hand column refers to a halftone mask with a half-pitch of 75 nm (1x) imaged with a quasar aperture at  $NA = 0.8$  and  $\sigma = 0.92$ .

negligible rotation match differences of  $C$ ,  $MaxTrans$ , and  $MinTrans$  allow for a reliable defect dispositioning of advanced masks independent on their pattern's orientation (horizontal or vertical). Also, the repeatability measurements demonstrate a significantly smaller  $3\sigma$ -variance compared to the AIMS fab 193SE tool. These improved characteristics can mainly be attributed to an improved hardware assembly of the AIMS fab 193i with an energy monitoring system maintaining the energy flux of each measurement at a constant level and with an improved homogenizing unit that keeps intensity variations within the  $\sigma$ -aperture and within the field at a low level. The results shown in this study demonstrate the capability of the AIMS fab 193i for reliable and reproducible defect dispositioning for state-of-the-art production masks below the 90 nm node with their tight defect specifications. The considerably reduced variances of the tool are a big leap from a defect dispositioning tool towards a defect metrology tool. It will be interesting to investigate the behavior of the tools with respect to CD evaluation and the impact of aberrations on these evaluation technique. In addition, along with the higher throughput of the current (AIMS fab 193i) and upcoming (AIMS 45-193i) AIMS systems a challenge for future system improvements would be automated data evaluation being standard for metrology tools.

## ACKNOWLEDGMENTS

The authors wish to thank Martin Stengl, Thomas Thaler, and Falk Hoffmann for their help in taking AIMS images.

## REFERENCES

1. A. C. Dürr, K. Bubke, M. Sczyrba, S. Angonin, "The importance of being homogeneous: on the influence of illumination inhomogeneity on AIMS images", Proc. SPIE Vol. 5992, p. 859-872, 2005.
2. A. M. Zibold, R. Schmid, K. Böhm, R. Brunner, A. C. Dürr, "Application results at 193nm: lithography emulation by aerial imaging and supplementary high resolution measurements", Proc. SPIE Vol. 5835, p. 115-121, 2005.

3. A. M. Zibold, E. Poortinga, H. v. Doornmalen, R. Schmid, T. Scherübl, W. Harnisch, "Advances with the new AIMS fab 193 2nd generation: a system for the 65 nm node including immersion", Proc. SPIE Vol. 5853, p. 371-379, 2005.
4. P. Dirksen, J. J. M. Braat, A. J. E. M. Janssen, C. A. H. Juffermans, "Aberration retrieval using the extended Nijboer-Zernike approach", Journal of Microlithography, Microfabrication, and Microsystems 2, pp. 61-68, 2003.
5. C. van der Avoort, J. J. M. Braat, P. Dirksen, A. J. E. M. Janssen, "Aberration retrieval from the intensity point-spread function in the focal region using the extended Nijboer-Zernike approach", J. Mod. Opt. 52, pp. 1695-1728, 2005.
6. J. J. M. Braat, P. Dirksen, A. J. E. M. Janssen, A. S. van de Nes, S. van Haver, "Extended Nijboer-Zernike approach to aberration and birefringence retrieval in a high-numerical-aperture optical system", J. Opt. Soc. Am. A. 22, pp. 2635-2650, 2005.